Electron Attachment to $(H_2O)_2Ar_n$ Clusters†

M.-K. Tsai, F. Wang,‡ and K. D. Jordan*

Department of Chemistry and Center for Molecular and Materials Simulations, University of Pittsburgh, Pittsburgh, Pennsylvania 15260

Received: October 11, 2003; In Final Form: November 28, 2003

The neutral and negatively charged $(H_2O)_2Ar_n$, $n = 1-14$, clusters are investigated theoretically by use of a polarizable model potential together, in the case of the anionic clusters, with a Drude-model approach to incorporate dispersion interactions between the excess electron and the argon atoms and water molecules. The $(H_2O)_2Ar_{11}$ and $(H_2O)_2^-Ar_{12}$ clusters are predicted to be "magic numbers", with their high stability being a result of their global minima adopting icosahedral-like structures. On the basis of these results, a mechanism for formation of the anions is proposed. In addition, the rapid falloff in intensity of the $n \geq 7$ anionic clusters in the observed mass spectrum and the absence of observable signal for the $n = 10$ cluster are accounted for.

I. Introduction

Negatively charged water clusters have been the subject of numerous experimental and theoretical studies.[1−15] Although the water monomer does not have a bound anion state, the dimer is a prototypical dipole-bound anion in which the excess electron is bound in a diffuse orbital "trapped" by the dipole field.[15−20] Experimentally, $(H_2O)_2^-$ ions were first produced by injection of low-energy electrons into the high-pressure region of a seeded supersonic expansion.[11,12] The diffuse nature of the excess electron orbital of $(H_2O)_2^-$ was first experimentally demonstrated by Haberland et al.,[11] who, using electron detachment in an external field, obtained an electron affinity of 17 meV. In these experiments, the supersonic beam was seeded with argon atoms to produce cold clusters. Subsequently, Bowen et al.[12] determined from photodetachment experiments a value of 45 ± 6 meV for the vertical electron detachment energy (VDE) of $(H_2O)_2^-$. They also observed weak HOH bending and OH stretching vibrational features indicative of a geometry change between the neutral and anionic dimers. Recently, Bouteiller et al.[13] reported an adiabatic electron affinity of $(H_2O)_2$ of 30 ± 4 meV from field-detachment of $(H_2O)_2^-$ anions produced by transfer of an electron from Rydberg helium atoms.

Theoretical studies have shown that while $(H_2O)_2$ has a *trans*-like structure the anion has a *cis*-like structure as shown in Figure 1. This geometrical change associated with electron capture is due to the larger dipole moment, and hence, enhanced electron binding for the cis orientation of the two water molecules. To a large extent the difference between the recent experimentally determined values of the VDE of $(H_2O)_2^-$ and of the adiabatic EA of $(H_2O)_2$ can be understood in terms of this geometry change.

As noted above, one way of preparing the fragile $(H_2O)_2^-$ species is via the interaction of an electron source with a co-expansion of water and argon. The seeding gas helps cool the $(H_2O)_2$ dimer, thereby suppressing vibrational hot bands and electron autodetachment. The co-expansion with argon also leads to mixed $(H_2O)_2^-Ar_n$ clusters. A representative mass spectrum

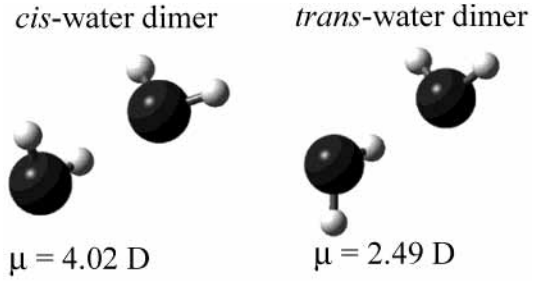

Figure 1. *cis*- and *trans*-$(H_2O)_2$. The cis structure is not a potential energy minimum in the absence of the excess electron. The dipole moments are from MP2/aug-cc-pVDZ calculations.

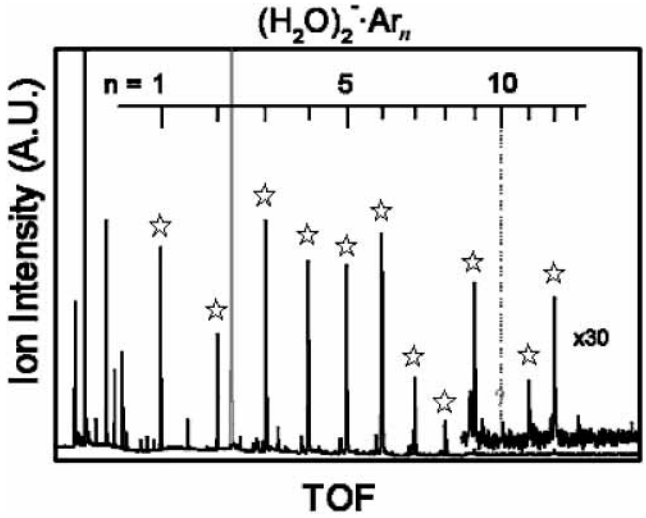

Figure 2. $(H_2O)_2^-Ar_n$ spectrum from M. A. Johnson (ref 21). The stars denote peaks due to $(H_2O)_2^-Ar_n$. The intense gray peak is due to I^-.

of $(H_2O)_2^-Ar_n$ determined by Ayotte and Johnson[21] is shown in Figure 2. The signals due to the $n = 1$ and 3−6 clusters are of roughly the same intensity, with that due to the $n = 2$ ion being roughly half as intense. There is a significant falloff in ion intensity for $n > 6$, with no detectable signal for $n = 10$, and with the $n = 9$ and 12 clusters appearing with much greater intensity than the $n = 11$, and 13−15 clusters.[21] Interestingly,

† Part of the special issue "Fritz Schaefer Festschrift".

* Corresponding author.

‡ Present address: Department of Chemistry, University of Utah, Salt Lake City, UT 84112-0850.

10.1021/jp037081g CCC: $27.50
Published on Web 01/17/2004

Corcelli et al.[22] have reported a mass spectrum of the $Cl^-\cdot H_2O\cdot Ar_n$, $n = 1-13$, clusters which displays intense peaks through $n = 11$ and low intensities for $n \geq 12$. This was interpreted in terms of icosahedral closing at $n = 11$ with the Cl^- ion occupying the center of the icosahedron and a H_2O molecule substituted at one position of the first solvation shell. This raises the question as to whether icosahedral-type arrangements might also play a role in establishing the intensity pattern in the mass spectrum of the $(H_2O)_2^-Ar_n$ clusters.

In this work, the potential energy minima and the finite temperature properties of the $(H_2O)_2Ar_n$ and $(H_2O)_2^-Ar_n$, $n \leq 14$, clusters are investigated theoretically. The goals of the calculations are 2-fold: (1) to develop a detailed understanding of how the Ar atoms impact the electron binding, and (2) to determine whether certain sized clusters are especially stable energetically and whether the observed ion-intensity pattern of $(H_2O)_2^-Ar_n$ reflects the relative stabilities of either the neutral or anionic clusters. Polarization and dispersion interactions between the excess electron and the Ar atoms necessarily act so as to enhance the electron binding. On the other hand, the presence of argon atoms in the region of space that would otherwise be "occupied" by the excess electron will tend to decrease the electron binding due to the exclusion of the excess electron from regions of space occupied by the Ar atoms (hereafter referred to as an "excluded volume" effect). With regard to the ion-intensity patterns, we recognize from the outset that factors other than energetics can influence cluster distributions. For example, the observation of a particular anion may depend on sufficiently rapid Ar evaporation (from a starting larger cluster) to suppress autoionization. Still there are many examples where it has been established that a mass spectral intensity distribution reflects primarily relative stabilities of the neutral or ionic clusters. One of the best known examples is carbon clusters, for which the fullerene members are especially intense in the positive ion mass spectrum.[23]

II. Computational Methodology

To accurately describe by use of ab initio methods the binding of an excess electron to clusters of polar molecules it is necessary to employ very flexible basis sets and to include electron correlations effects through high order.[15,24-26] As a result, geometry optimizations of the $(H_2O)_2^-Ar_n$, $n \geq 3$, clusters using suitable ab initio methods would be computationally prohibitive. In the present study, this problem is dealt with by use of a one-electron model for describing an excess electron interacting with the H_2O molecules and the Ar atoms.

A. Potential Model for the Neutral $(H_2O)_2Ar_n$ Clusters. The neutral $(H_2O)_2Ar_n$ clusters were described by combining a Lennard-Jones potential for the Ar−Ar interactions, the Dang-Chang (DC) model[27] for the water−water interactions, and the Cohen-Saykally potential[28] for the Ar−water interactions, together with additional terms, described below, to incorporate many-body polarization.

The parameters for the Ar−Ar Lennard-Jones potential ($\sigma = 3.405$ Å and $\epsilon = 0.996$ kJ/mol)[29] were taken from the literature. The DC water model employs the experimental geometry of the gas-phase monomer ($R_{OH} = 0.9572$ Å, HOH angle = 104.52°), with two point charges ($Q = 0.519$e) located at the positions of the H atoms and a third ($Q = -1.038$e) on the rotational axis, displaced 0.215 Å from the O atom (toward the H atoms). This point-charge distribution gives for H_2O a dipole moment of 1.848 D, nearly identical to the experimental value of 1.825 D[30] and quadruple moment components of $Q_{xx} = 2.235$ D·Å, $Q_{yy} = -2.047$ D·Å, and $Q_{zz} = -0.188$ D·Å, in good agreement with experimental values.[31] (Here it is assumed that the molecule is oriented in the *xz* plane, with the rotational axis being the *z* axis.) The DC model also locates an isotropic polarizable site at the same position as the negative charge, with the polarizability chosen to reproduce the experimental value. Finally, a single Lennard-Jones site is located on the O atom ($\sigma = 3.2340$ Å and $\epsilon = 0.763$ kJ/mol).

The Cohen-Saykally Ar−water potential is of the following form:

$$V(R,\theta,\phi) = V^{rep}(R,\theta,\phi) - \sum_{n=6}^{9} C_n^{ind}(\theta,\phi)R^{-n} - \sum_{n=6}^{9} C_n^{disp}(\theta,\phi)D_n(R)R^{-n} \quad (1)$$

where V^{rep} represents the short-range repulsive interaction C_n^{ind} and C_n^{disp} are the inductive and dispersion coefficients, respectively, and the D_n are damping factors. The various parameters were determined by fitting the parameters to 37 vibration−rotation−tunneling transitions observed for the ArH_2O and ArD_2O complexes, subject to constraints to build in the correct long-range behavior.[28] This potential includes through the C_n^{ind} terms a contribution due to the polarization of the Ar atom by the dipole and quadrupole moments on the water monomers.

To include many-body polarization in the composite model described above, Drude oscillators were placed on the Ar atoms and were also substituted for the polarizable site in the DC model for each of the water monomers. Each Drude oscillator consists of two charges ($+q$ and $-q$) coupled harmonically through a force constant k. The polarizability of a Drude oscillator is given by q^2/k (in atomic units). For water, the k and q values were taken from ref 24 ($k = 0.103$, and $q = 1$, for which q^2/k value reproduces the polarizability value of the DC model). For Ar, k and q were chosen to be 0.395 and 2.086, respectively. With this choice, q^2/k reproduces the experimental polarizability of Ar, and the dispersion energy of Ar_2 calculated using the Drude model closely reproduces the contribution from the R^{-6} term in the Lennard-Jones potential (over the distance range of $R = 3-8$ Å). The many-body polarization interactions were calculated using the standard approach,[22]

where

$$U^{pol} = U_{qp} + U_{pp} + U_{self} \quad (2)$$

with

$$U_{qp} = -\left(\sum_{i=1}^{N_W} p_i^W \cdot E_i^0 + \sum_{k=1}^{N_{Ar}} p_k^{Ar} \cdot E_k^0\right) \quad (3)$$

$$U_{pp} = -\frac{1}{2}\left(\sum_{i=1}^{N_W}\sum_{j=1,j\neq i}^{N_W} p_i^W \cdot T_{ij}\, p_j^W + \sum_{k=1}^{N_{Ar}}\sum_{l=1,k\neq l}^{N_{Ar}} p_k^{Ar} \cdot T_{kl} \cdot p_l^{Ar}\right) \quad (4)$$

$$U_{self} = \sum_{i=1}^{N_W} \frac{p_i^W \cdot p_i^W}{2\alpha_i^W} + \sum_{k=1}^{N_{Ar}} \frac{p_k^{Ar} \cdot p_k^{Ar}}{2\alpha_k^{Ar}} \quad (5)$$

where U_{qp} describes the interaction energy between the induced dipoles and the electric fields from the permanent charges on other sites, U_{pp} is the interaction energy between the induced dipoles, and U_{self} is the energy needed to create the induced dipoles. In these expressions, E_i^0 is the electric field at polarizable site i due to the permanent charges from the other sites (the charges associated with a water monomer do not

interact directly with the polarizable site associated with that monomer), α_i and p_i are, respectively, the polarizability and induced dipole associated with site i, N_W and N_{Ar} are, respectively, the number of water molecules and Ar atoms, and T_{ij} is the dipole tensor.

Because the Cohen-Saykally potential already incorporates two-body polarization interactions between water molecules and Ar atoms, one has to be careful to avoid double counting of such interactions when combining it with Drude oscillators to incorporate many-body polarization. The obvious approach for avoiding the double counting would be to eliminate the polarization contribution from the Cohen-Saykally potential. However, polarization and dispersion are not cleanly separable in that potential. For that reason, we adopted an alternative strategy of excluding from eq 3, the interaction of the Drude oscillators on the Ar atoms with the field due to the charges on the water molecules (and the associated self-energy term in eq 5). We do calculate the induced dipoles on the Ar atoms due to the electric field from the water molecules and use these to include induced dipole−induced dipole interactions between Ar atoms. Although, this approach does omit a subset of the many-body interactions involving both water molecules and the Ar atoms, the errors due to the neglect of these terms are quite small.

To treat the negatively charged clusters, the model potential described above was combined with the Hamiltonian

$$H^e + V^{couple} \tag{6}$$

where H^e is the one-electron Hamiltonian,

$$H^e = -\frac{1}{2}\nabla_e^2 + \sum_i \frac{Q_i}{r_i} + \sum_i \frac{\mu_i \cdot r_i}{r_i^3} + V^{exch-rep} \tag{7}$$

and V^{couple} gives the coupling between the excess electron and the Drude oscillators. In eq 7, the Q_i are the permanent charges associated with the water monomers, and the μ_i are induced dipoles associated with the Ar atoms and the water monomers obtained from solution of eqs 3−5. $V^{exch-rep}$ describes the short-range repulsive interactions between the excess electron and the Ar atoms and water molecules. The electron−Ar repulsive potential was taken to be the three *s*-type Gaussian representation of Space et al.,[29] and the electron−H_2O repulsive potential was taken from a recent paper of Wang and Jordan.[32]

The electron−Drude oscillator coupling is defined as

$$V^{couple} = \sum_j \frac{q_j R_j \cdot r_j}{r_j^3} f(r_j) \tag{8}$$

where r_j is a vector between the excess electron and the center of the jth Drude oscillator, R_j is the vector locating the negative charge of the jth oscillator relative to the associated positive charge, and $f(r_j)$ damps out the unphysical short-range interactions, with the damping function for the coupling of the excess electron with Drude oscillators associated with the water monomers being taken from ref 32 and that for the coupling of the excess electron to the Drude oscillators associated with the Ar atoms being determined in this study. The Schrödinger equation associated with eq 7 was solved using a large flexible Gaussian-type orbital to describe the excess electron. A product basis set was then constructed using these one-electron orbitals and harmonic oscillator functions to describe each of the Drude oscillators, and this basis set was used in calculating the electron binding energies associated with the full Hamiltonian (eq 6) and using the configuration interaction (CI) method.

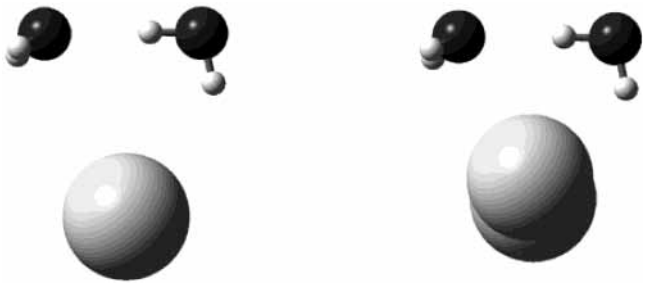

Figure 3. Second lowest-energy isomers of *cis*-$(H_2O)_2^-Ar$ and *cis*-$(H_2O)_2^-Ar_2$.

B. Geometry Optimizations. Analytical gradients have not been worked out for the model potentials used to describe the neutral and anionic $(H_2O)_2Ar_n$ clusters. For this reason, geometries were optimized using the simulated annealing[33] and Powell algorithms[34] as described below.

The geometries of the neutral clusters were optimized for both "cis" and "trans" orientations of the water dimer as shown in Figure 1. In these calculations, the geometries of the $(H_2O)_2$ portions of the mixed $(H_2O)_2Ar_n$ and $(H_2O)_2^-Ar_n$ clusters were taken from MP2 optimizations on the isolated $(H_2O)_2$ and $(H_2O)_2^-$ species, with the OH bond lengths and the HOH angles of the monomers constrained to the experimental values for an H_2O monomer.

The starting structures of the *trans*-$(H_2O)_2Ar_n$ clusters were generated by placing the Ar atoms at random locations in a sphere of radius 3.6−9 Å, with the size of the sphere growing with the number of atoms, and its origin being taken as the center-of-mass of the water dimer. For the *cis*-$(H_2O)_2Ar_n$ clusters, three different choices were made for the initial locations of the Ar atoms. The first choice followed the same procedure as used the *trans*-$(H_2O)_2Ar_n$ clusters. The second placed the Ar atoms in the vicinity of the H-donor water molecule. The third choice restricted the initial positions of the Ar atoms to the half sphere opposite the free OH groups. This last choice was motivated by the use of the local minima of the neutral clusters for starting the anion optimizations and by the realization that the presence of Ar atoms near the free OH groups can prevent electron binding due to an "excluded-volume" effect. To demonstrate the latter effect, we consider *cis*-$(H_2O)_2^-Ar$ and *cis*-$(H_2O)_2^-Ar_2$. Drude-model calculations predict the most stable forms of these two cluster anions to have structures with the Ar atoms located opposite the free OH groups and with vertical electron detachment energies of 3.2 and 3.0 kJ/mol. There are also higher-lying local minima, shown in Figure 3, with the Ar atoms on the same side of the water dimer as the free OH groups. For these isomers the vertical electron detachment energies are calculated to be only 0.6 and 0.2 kJ/mol for $(H_2O)_2^-Ar$ and $(H_2O)_2^-Ar_2$, respectively. As an increasing number of Ar atoms are located in the vicinity of the free OH groups, the excess electron becomes so weakly bound that, were corrections to the BO approximation made, the electron would cease to be bound even though the dipole moment is larger than the "critical" dipole moment.

The initial temperature of the simulated annealing procedure was chosen to be 35 K which should be high enough that the barriers on the potential energy surface are readily overcome but low enough to avoid evaporation (at least for the duration of the calculations). It is relevant to observe that a recent simulation of $Ar_{12}HF$ gave two peaks in the heat capacity curve.[35] The first peak near $T = 11$ K corresponds to the

TABLE 1: Relevant Energies (kJ/mol)[a]

Ar−Ar binding energy	−1.00
water−water binding energy (trans)	−19.22
Ar−water binding energy	−1.71
VDE of *cis*-$(H_2O)_2^-$	3.33
VDE of *trans*-$(H_2O)_2^-$	0.03
trans → cis isomerization energy of $(H_2O)_2$	2.05
trans → cis isomerization energy of $(H_2O)_2^-$	−0.98

[a] All results obtained using the model potentials described in the text.

migration of the HF molecule from the center of the cluster to the surface, and the second peak near $T = 30$ K corresponds to melting of the cluster. It is anticipated, therefore, that the Ar atoms should be quite mobile at the 35 K initial temperature used to start the simulated annealing optimizations.

For each $(H_2O)_2Ar_n$ cluster with a trans arrangement of the water molecules, 100 optimizations starting from different initial structures were carried out. For the cis clusters, 300 separate optimizations, 100 for each of the three ways of initially locating the Ar atoms, were carried out. The strategy for the optimizations was closely modeled after that used by Corcelli et al.[22] in their study of $Cl^-H_2OAr_n$ clusters and proceeded as follows:

1. Starting from a given initial structure, a Monte Carlo simulation was carried out for 1000 cycles at $T = 0.05$ K to give compact structures to avoid evaporation in the subsequent annealing. (A cycle corresponds to one sweep through all the argon atoms.)

2. Starting with the structure obtained from step 1, the cluster was annealed from 35 to 1 K, in 0.5 K decrements, with 1000 Monte Carlo cycles being performed at each temperature.

3. Starting at 1 K, the temperature was decreased by a factor of 2 every 500 cycles down to a temperature of 10^{-6} K.

The Monte Carlo steps were carried out with the Metropolis procedure,[36] with the maximum displacements being dynamically adjusted to maintain close to a 50% acceptance rate. Moves that placed Ar atoms within 2 Å of the mass center of the water dimer were rejected.

An analogous optimization approach for the anionic clusters would have been computationally prohibitive even with the use of the Drude model. For that reason we chose instead to optimize the anionic clusters using the Powell[34] procedure starting from each unique structure obtained from the simulated annealing optimizations of the *cis*-$(H_2O)_2Ar_n$ clusters.

In addition to the geometry optimizations described above, Monte Carlo simulations in the canonical ensemble were carried out for the neutral $(H_2O)_2Ar_n$ clusters at a temperature of 35 K, which is believed to be close to that of the clusters produced experimentally.[37] Actually, clusters with an internal energies in excess of that required to evaporate an argon have finite lifetimes, which makes a rigorous characterization by temperature questionable. This problem was avoided in our simulations by imposing a constraining region comprised of two overlapping spheres centered on the O atoms. The sphere radii ranged from 6.5 Å for $n = 1$ to 13.5 Å for $n = 14$. These simulations employed frozen geometries for the water monomers and a fixed O−O distance, but allowed for cis−trans isomerization of the water dimer. The simulations consisted of an equilibration stage, followed by 5 000 000 production moves. The geometries were stored every 1000 moves. For each saved structure, the energy of the anion was calculated.

III. Results

Before examining the results of the calculations, it is instructive to review the key interaction energies (see Table 1).

TABLE 2: Vertical Electron Detachment Energies (kJ/mol) and Computational Times for $(H_2O)_2^-Ar_n$, $n = 0-2$

	cis-$(H_2O)_2^-$	*cis*-$(H_2O)_2Ar^-$	*cis*-$(H_2O)_2Ar_2^-$
		CCSD(T)	
VDE	3.20	3.63	4.24
CPU time	1.6 h	31.0 h	111.5 h
		Drude model	
VDE	3.33	3.62	4.62
CPU time	1.3 s	2.1 s	3.2 s

The binding energy of Ar−H_2O is calculated to be −1.7 kJ/mol as compared with the −1.0 kJ/mol binding energy of the argon dimer, and the 3.33 kJ/mol VDE of *cis*-$(H_2O)_2^-$. Although the energy for converting $(H_2O)_2$ from its "trans" global minimum structure to the "cis" structure is calculated to be 2.0 kJ/mol, the cis form of $(H_2O)_2^-$ is calculated to be about 1.0 kJ/mol more stable than the trans form. This can be understood in terms of the enhanced dipole moment of the cis structure, which leads to greater electron binding.

To examine the quality of the model potential, we also carried out ab initio CCSD(T) calculations[38] of the vertical electron detachment energies of $(H_2O)_2Ar_n^-$, $n = 0-2$, clusters using the anion geometries optimized with the one-electron Drude model and with the water monomers held rigid in the cis orientation. The ab initio calculations were carried out using a basis set generated by adding to a modified aug-cc-pVTZ(-f) basis set,[39,40] seven diffuse *s* and seven diffuse *p* primitive Gaussian functions on the O atom of the acceptor water molecule. The exponents of the supplemental functions were in geometric ratios, ranging from 0.025 to 4×10^{-5} for the *s* functions and from 0.06 to 9.6×10^{-5} for the *p* functions. (The modification of the aug-cc-pVTZ basis set consisted of substituting for the H and O atoms, respectively, the *p* and *d* functions from the aug-cc-pVDZ basis set.[41] In addition, the *f* functions on the O atoms and the *d* functions on the H atoms, present in the full aug-cc-pVTZ basis set were excluded, hence the "-f" qualifier.) The electron binding energies are summarized in Table 2. For $(H_2O)_2^-$ and $(H_2O)_2^-Ar$ the model potential and the ab initio calculations give nearly identical vertical electron detachment energies, but for $(H_2O)_2^-Ar_2$, the value of the VDE obtained with the model potential is about 10% (0.4 kJ/mol) greater in magnitude than that obtained from the ab initio CCSD(T) calculations. However, even in the later case the agreement between the model potential and high-level ab initio results is satisfactory.

A. Neutral $(H_2O)_2Ar_n$ Clusters. The lowest-energy minima of the neutral *trans*-$(H_2O)_2Ar_n$ and *cis*-$(H_2O)_2Ar_n$ clusters are depicted in Figures 4−6. For each cluster size, the trans isomer is 2.0−2.3 kJ/mol more stable than the cis isomer, with this energy difference being close to that to associated with isomerization of the bare water dimer. The most stable forms of the *trans*-$(H_2O)_2Ar_n$, $n = 1-3$, clusters have the Ar atoms located on the same side of the O−O bond as the free OH group of the acceptor monomer. However, the larger trans clusters have Ar atoms on both sides of the O−O bond. The five Ar atoms of *trans*-$(H_2O)_2Ar_5$ form a ring around the O−O axis. This five-membered ring persists in the larger clusters. For the most stable forms of the *cis*-$(H_2O)_2Ar_n$, $n = 1-3$, 5, and 6, clusters the Ar atoms are located on the side of the O−O bond opposite the free OH groups, whereas in the other cis clusters there are Ar atoms on both sides of the O−O bond. (Here the "sides" are defined respect to the plane containing the two O atoms and which is perpendicular to the plane containing the two O atoms and the free OH group of the donor water molecule.)

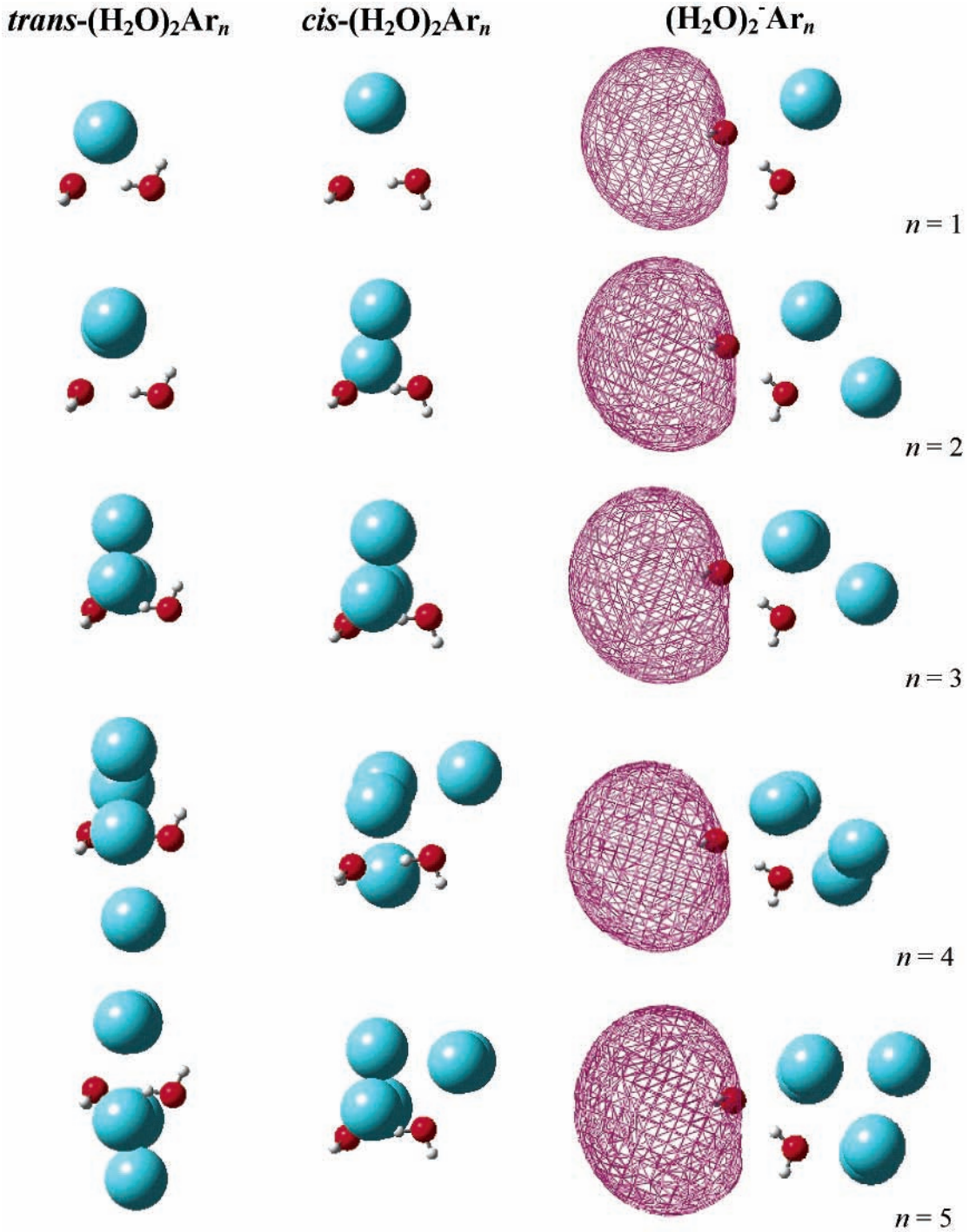

Figure 4. Lowest-energy minima of the *trans*-$(H_2O)_2Ar_n$, *cis*-$(H_2O)_2Ar_n$, and $(H_2O)_2^-Ar_n$, $n = 1-5$, clusters. The neutral clusters were optimized by use of the simulated annealing procedure and the anionic clusters by means of the Powell algorithm. For the anions, the orbital occupied by the excess electron in the isolated $(H_2O)_2^-$ ion is depicted.

For both the *cis*- and *trans*-$(H_2O)_2Ar_n$ clusters, the incremental binding energy per Ar atom undergoes a sizable jump in magnitude in going from the $n = 10$ to the $n = 11$ cluster. (See Figure 7.) This is a consequence of the $n = 11$ cluster adopting an icosahedral-like structure, with one water molecule occupying the center site and the other a surface site of the approximate icosahedron.

B. $(H_2O)_2^-Ar_n$ Clusters. Figures 4−6 also show the lowest-energy structures of the anionic clusters, and the associated binding energies are summarized in Table 3. In each anionic cluster, the water dimer is on the surface of the argon cluster with the OH groups of the acceptor monomer (that to which the excess electron binds) pointing away from the argon cluster. The $n = 11$ and 12 anionic clusters display the largest incremental binding energies per Ar atom, with the change being greater for the $n = 12$ cluster. (See Figure 7.) The high stability of $(H_2O)_2^-Ar_{12}$ is due to its adopting an icosahedral-like structure, with the single-donor water molecule occupying one of the sites on the surface of the icosahedron. The most stable forms of the $n = 11$ and 13 anionic clusters have structures closely related to that of the $(H_2O)_2^-Ar_{12}$ species. The evolution of the icosahedral structure is apparent starting at the $n = 5$

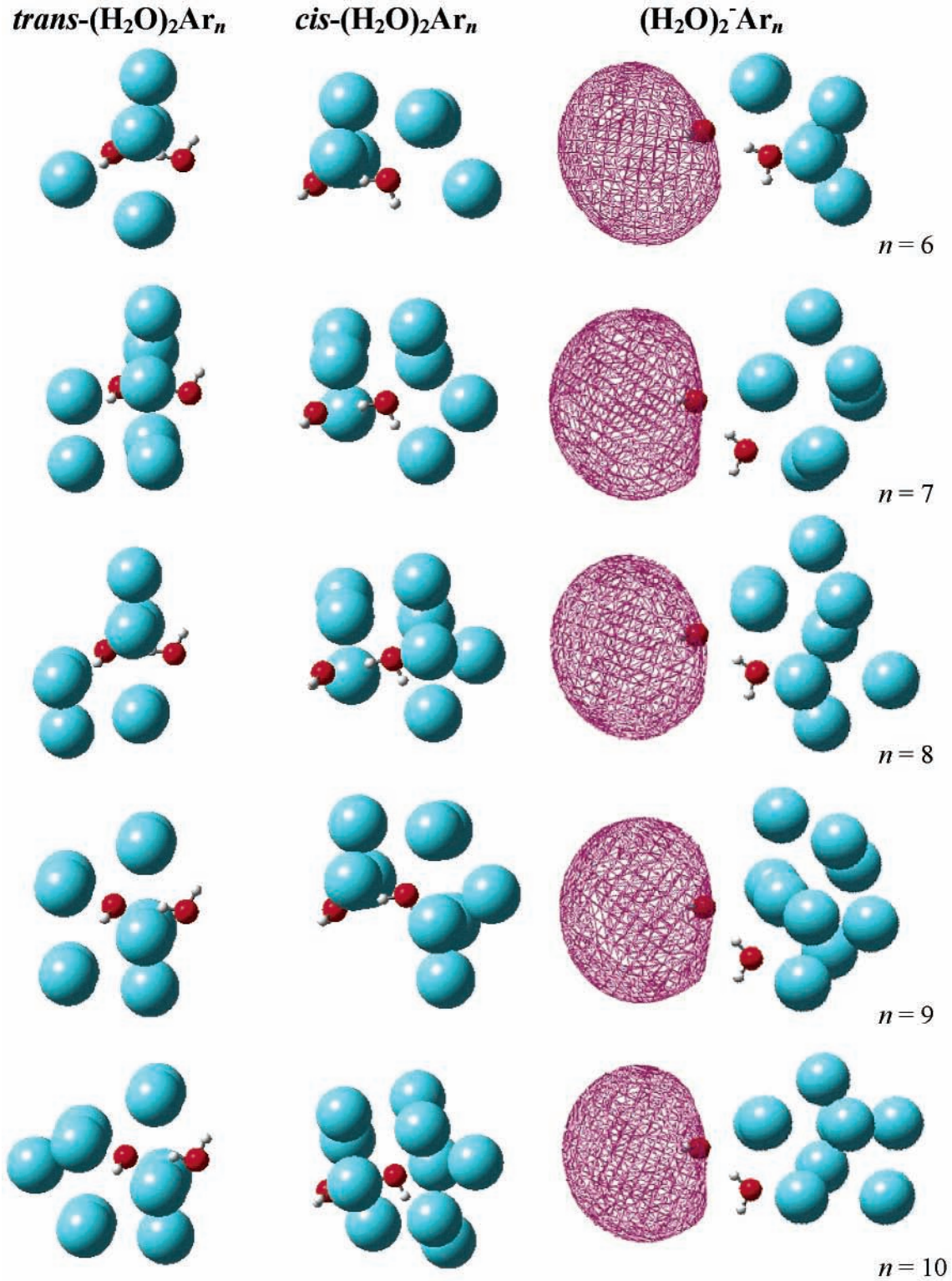

Figure 5. Lowest energy minima of the *trans*-$(H_2O)_2Ar_n$, *cis*-$(H_2O)_2Ar_n$, and $(H_2O)_2^-Ar_n$, $n = 6-10$, clusters. The neutral clusters were optimized by use of the simulated annealing procedure and the anionic clusters by means of the Powell algorithm. For the anions, the orbital occupied by the excess electron in the isolated $(H_2O)_2^-$ ion is depicted.

cluster. We note also that for the $n = 13$ cluster there is an isomer with an intact Ar_{13} icosahedron "attached" to the H-donor water molecule lying only 1.2 kJ/mol above the global minimum structure.

For $(H_2O)_2^-Ar_n$, $n = 0-6$, clusters the most stable form of the anion lies energetically below the most stable form of the neutral cluster, which implies that for these clusters the electron binding more than compensates for the energy required to isomerize the water dimer from trans to cis together with that required to rearrange the Ar atoms. On the other hand, for the larger clusters, the combined energy cost for isomerizing the water dimer and rearranging the Ar atoms exceeds the electron binding, with the consequence that the $n \geq 7$ clusters have negative adiabatic electron affinities.

C. Monte Carlo Simulations. Table 4 reports for the $(H_2O)_2Ar_n$ clusters the average energies and the numbers of saved

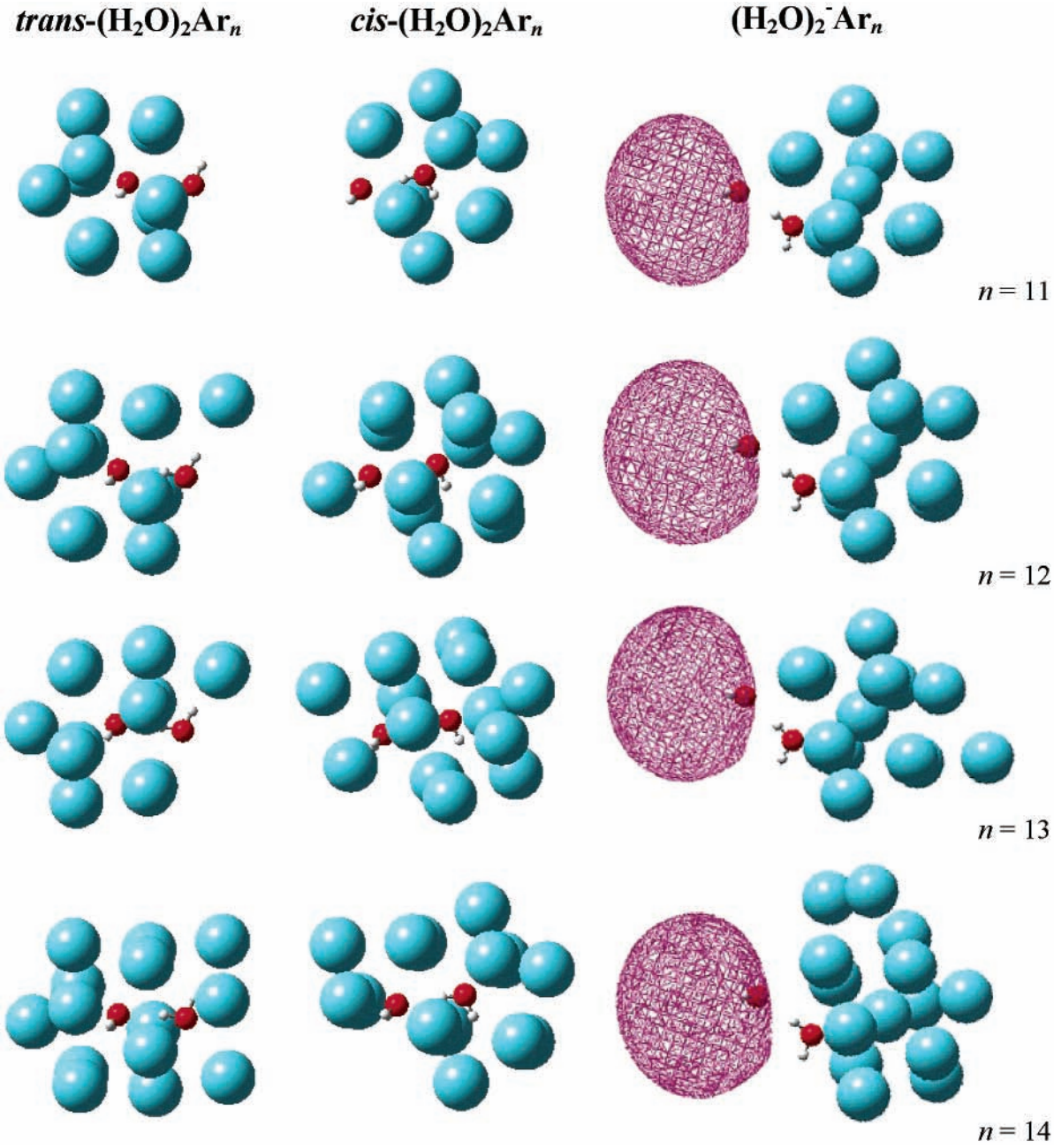

Figure 6. Lowest energy minima of the *trans*-$(H_2O)_2Ar_n$, *cis*-$(H_2O)_2Ar_n$, and $(H_2O)_2^-Ar_n$, $n = 11-14$, clusters. The neutral clusters were optimized by use of the simulated annealing procedure and the anionic clusters by means of the Powell algorithm. For the anions, the orbital occupied by the excess electron in the isolated $(H_2O)_2^-$ ion is depicted.

configurations from the 35 K Monte Carlo simulations that have electron binding energies greater than 0.26 kJ/mol in magnitude. Clusters with electron binding energies less than about 0.26 kJ/mol in the Born−Oppenheimer approximation are expected not to bind the electron were corrections to the BO approximation included. The number of sampled configurations capable of binding an excess electron (according to the above definition) drops off rapidly with increasing of Ar atoms, and for the $n \geq 9$ clusters, none of the sampled configurations displayed electron binding (based on the 0.26 kJ/mol threshold). Nonetheless, as may be seen from Figure 8, at $T = 35$ K the neutral cluster does sample configurations that expose the acceptor water molecule and with the water dimer well along the coordinate for trans → cis isomerization. Even though these structures have BO electron binding energies less than 0.26 kJ/mol, the distortions induced by the incoming electron could lead to appreciable electron binding.

The $(H_2O)_2^-Ar_n$ clusters observed mass spectroscopically are unlikely to derive from the "parent" $(H_2O)_2Ar_n$ clusters. This is on account of the fact that the resulting anions would be subject to rapid electron autoionization. The most likely mechanism for stabilization of the anions against electron detachment is via evaporative loss of an Ar atom,

$$(H_2O)_2Ar_n + e^- \rightarrow (H_2O)_2^-Ar_n \rightarrow (H_2O)_2^-Ar_{n-1} + Ar \quad (9)$$

The energetics involved in this process can be understood from examination of Figure 9, which reports the potential energy distributions calculated for a subset of the neutral clusters at $T = 35$ K, as well as the thresholds for formation of $(H_2O)_2^-Ar_{n-1}$ and of $(H_2O)_2Ar_{n-1}$.

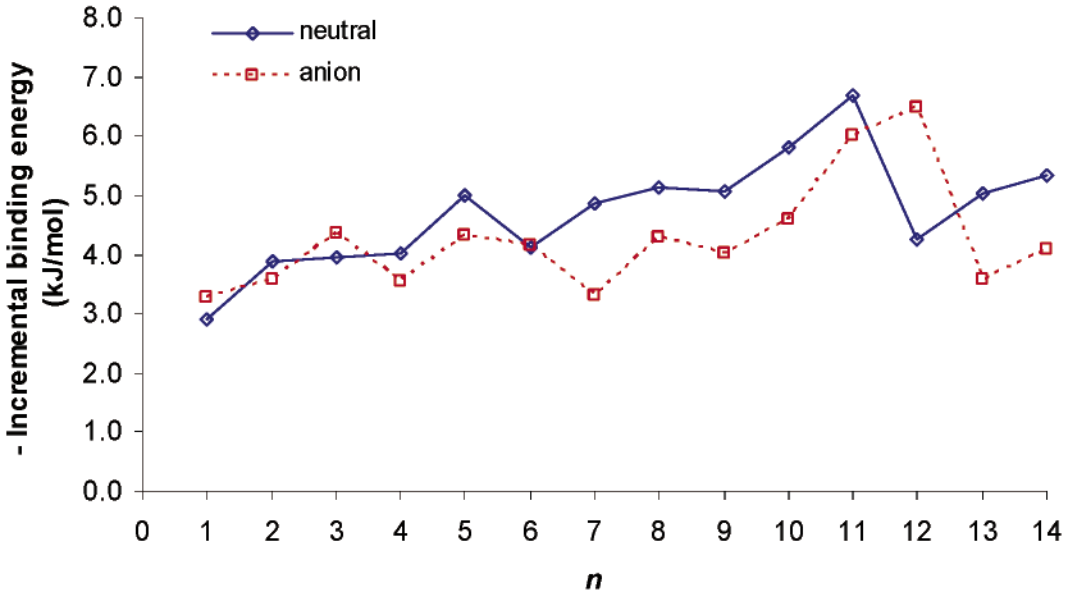

Figure 7. Incremental binding energy, $\Delta E_n^\circ = E[(H_2O)_2Ar_n] - E[(H_2O)_2Ar_{n-1}]$ and $\Delta E_n^- = E[(H_2O)_2^-Ar_n] - E[(H_2O)_2^-Ar_{n-1}]$, of the *trans*-$(H_2O)_2Ar_n$ and *cis*-$(H_2O)_2Ar_n^-$, $n = 1-14$, clusters.

TABLE 3: Total Energies (kJ/mol) of the Most Stable Forms of the Neutral and Anionic $(H_2O)_2Ar_m$ Clusters

	trans-$(H_2O)_2Ar_m$[a]		*cis*-$(H_2O)_2Ar_m$[a]		$(H_2O)_2^-Ar_m$		
m	E_{tot}	ΔE_m[b]	E_{tot}	ΔE_m[b]	E_{tot}	ΔE_m[b]	VDE
0	−19.22		−17.18		−20.51		3.33
1	−22.11	−2.89	−20.16	−2.99	−23.79	−3.28	3.65
2	−25.99	−3.88	−24.05	−3.88	−27.36	−3.57	4.62
3	−29.94	−3.96	−28.04	−3.99	−31.71	−4.35	4.35
4	−33.97	−4.02	−31.94	−3.90	−35.24	−3.53	4.53
5	−38.95	−4.99	−36.73	−4.78	−39.55	−4.31	5.03
6	−43.05	−4.10	−40.83	−4.11	−43.72	−4.17	4.50
7	−47.91	−4.85	−45.66	−4.83	−47.02	−3.30	5.37
8	−53.03	−5.13	−50.77	−5.11	−51.30	−4.28	4.94
9	−58.11	−5.08	−55.91	−5.14	−55.33	−4.03	5.06
10	−63.91	−5.80	−61.82	−5.91	−59.92	−4.58	5.37
11	−70.59	−6.69	−68.48	−6.66	−65.94	−6.02	5.39
12	−74.85	−4.26	−72.69	−4.21	−72.42	−6.48	5.59
13	−79.89	−5.03	−77.74	−5.06	−76.00	−3.59	5.59
14	−85.22	−5.34	−82.89	−5.15	−80.08	−4.08	6.02

[a] The $(H_2O)_2Ar_m$ clusters were optimized by simulated annealing with the geometries of the $(H_2O)_2$ portions of the clusters kept frozen. The anionic clusters were optimized with the Powell algorithm with the geometry of the $(H_2O)_2^-$ entity frozen at that of the isolated $(H_2O)_2^-$ ion. [b] $\Delta E_m = E_m - E_{m-1}$.

Examination of the potential energy distributions reveals that in all cases the threshold for the electron capture followed by Ar atom loss (eq 9) occurs at an energy at which the neutral cluster has sizable population (assuming a cluster temperature of 35 K). Moreover, for the $n \geq 7$ clusters the threshold for this channel lies energetically below that for

$$(H_2O)_2Ar_n + e^- \rightarrow (H_2O)_2^-Ar_n \rightarrow (H_2O)_2Ar_{n-1} + Ar + e^- \quad (10)$$

which is simply a consequence of the $n \leq 6$ clusters having positive electron affinities. As a result, for a subset of the $(H_2O)_2^-Ar_n$, $n \leq 6$, clusters formed by the electron capture/Ar atom evaporation channel (eq 9) further decay by either electron detachment or loss of a second Ar atom is not feasible energetically.

On the other hand, all $n \geq 7$ anionic clusters formed by the mechanism described by eq 9, are subject to electron autoionization. We believe that this explains the rapid falloff in anion intensity for the $n \geq 7$ clusters as well as the correlation between the intensity of the $n - 1$ ion signal in the mass spectrum and the excess energy that must be present in an $(H_2O)_2Ar_n$ cluster

TABLE 4: The Average Total Energies (kJ/mol) of the Neutral $(H_2O)_2Ar_m$ Clusters at 35 K,[a] and the Number of Structures Binding an Excess Electron

m	average energy	number of configurations binding an excess electron[b]
0	−18.68	2752
1	−21.02	828
2	−23.97	333
3	−27.24	117
4	−30.61	27
5	−34.21	15
6	−38.01	6
7	−41.93	2
8	−46.46	3
9	−51.11	0
10	−56.21	0
11	−62.54	0
12	−66.08	0
13	−70.46	0
14	−74.39	0

[a] The simulations employed rigid water monomers and fixed O−O distances. [b] Out of a total of 5000 configurations saved from the Monte Carlo simulation of the neutral cluster. A structure is counted as binding an excess electron if the calculated vertical electron detachment energy is ≥0.26 kJ/mol.

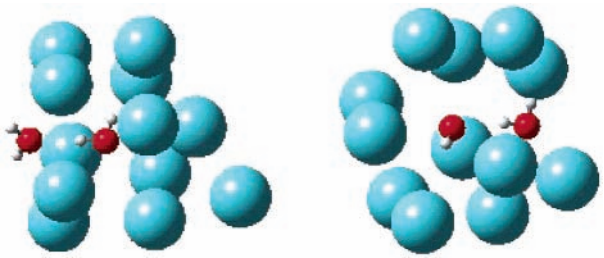

Figure 8. Snapshot configurations of $(H_2O)_2Ar_{12}$ from the $T = 35$ K Monte Carlo simulation. In the configuration on the left the water dimer is about halfway between the trans and cis arrangements. This configuration would require only a small rearrangement of Ar atoms to bind an excess electron. The configuration on the right would require extensive rearrangement of the Ar atoms to bind an electron.

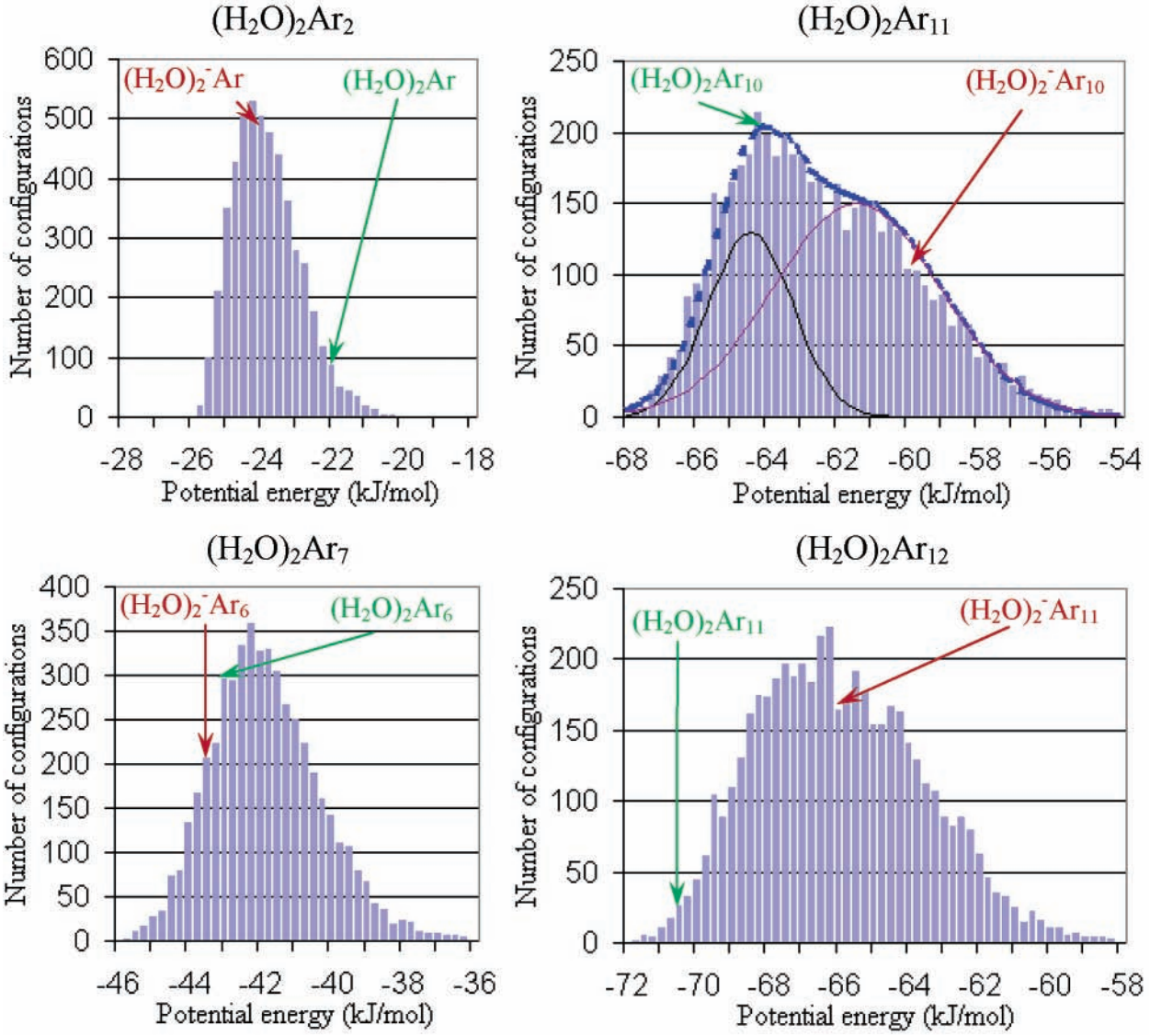

Figure 9. Potential energy distributions of the $(H_2O)_2Ar_n$, $n = 2, 7, 11, 12$, clusters at $T = 35$ K. The potential energies have been binned, with the individual bins reporting the number of saved configurations with energy between $E - 0.25$ and E in kJ/mol. The arrows report the threshold energies for forming the neutral and anionic $n - 1$ clusters. For $(H_2O)_2Ar_{11}$, the net distribution has been decomposed into two overlapping Gaussian distributions. The bordered columns correspond to the numbers of potential energy marked along *x*-axis.

for accessing the threshold for formation of $(H_2O)_2^-Ar_{n-1}$. With regard to the latter, the calculations predict the largest excess energies to be for the $n = 11$ and 14 clusters, (10.7 and 9.2 kJ/mol, respectively) which is expected to cause more rapid electron autoionization and could account for the absence (or only very weak signals) for $(H_2O)_2^-Ar_{10}$ and $(H_2O)_2^-Ar_{13}$ in the mass spectrum.

The energy at which the electron capture/Ar evaporation channel opens up is potentially relevant for a second reason, namely, the greater the excess energy in a neutral cluster, the shorter its lifetime toward evaporative loss of an Ar atom. It is estimated that under the experimental conditions used to obtain the mass spectrum reported in Figure 2, the time between formation of a neutral $(H_2O)_2Ar_n$ cluster and the initial electron capture event is on the order of microseconds.[42] Weerasinghe and Amar have studied using molecular dynamics simulations the lifetimes of the Ar_n, $12 \leq n \leq 14$, clusters as a function of excess energy.[43] These calculations give cluster lifetime on the order of nanoseconds for excess energies on the order of 20 kJ/mol. Based on the present calculations, the largest excess energy required for the opening up of the electron capture/Ar atom loss channel is 10.7 kJ/mol [in the case of $(H_2O)_2Ar_{11}$]. Molecular dynamics calculations carried out by us lead to average lifetimes of microseconds in this case. Thus, the lack of signal due of $(H_2O)_2^-Ar_{10}$ appears not to be due to the absence of $(H_2O)_2Ar_{11}$ precursor with sufficient excess energy to access the electron capture/Ar evaporation channel.

The potential energy distributions obtained from the MC simulations for $(H_2O)_2Ar_{11}$ and $(H_2O)_2Ar_{12}$ clusters are bimodal, which indicates the coexistence of solidlike and liquidlike phase at $T = 35$ K. This was an expected result, since simulations of Ar_{13} predict "solid−liquid" coexistence over a temperature range of 24−41 K with a pronounced peak in its heat capacity curve with a maximum at 34 K. Similar transitions have been predicted for the Ar_n, $n = 10-12$, clusters, but at somewhat lower temperatures.[44,45]

IV. Conclusions

In this investigation, the neutral and anionic $(H_2O)_2Ar_n$, $n = 0-14$, clusters have been characterized by means of model potentials, with explicit treatment of the excess electron in the case of the anionic clusters. The lowest-energy forms of $(H_2O)_2$-

Ar_{11} and $(H_2O)_2^-Ar_{12}$ are predicted to be especially stable and to have icosahedral-like structures. The adiabatic EA is predicted to be positive for the $n \leq 6$ clusters, but negative for the larger clusters. Both the finite temperature of the neutral cluster and distortions induced by the incoming electron appear to be important in the electron capture process. Moreover, we have proposed that the observed anions have one fewer Ar atom than their neutral precursors, i.e., that the initial electron capture event is followed by rapid ejection of an Ar atom. This provides a mechanism for formation of $(H_2O)_2^-Ar_n$, $n \leq 6$, clusters that are stable against electron ejection or further loss of Ar atoms. On the other hand, the $(H_2O)_2^-Ar_n$, $n \geq 7$, clusters formed by this process are still subject to electron autoionization. This apparently accounts for the rapid falloff in intensity in the $(H_2O)_2^-Ar_n$ mass spectrum for $n \geq 7$. In addition, it is suggested that the absence of signal due to the $(H_2O)_2^-Ar_{10}$ and $(H_2O)_2^-Ar_{13}$ clusters could be due to the rapid autoionization rates of the precursor $(H_2O)_2^-Ar_{11}$ and $(H_2O)_2^-Ar_{14}$ clusters.

V. Acknowledgments

This research was carried out with support from National Science Foundation. We thank Prof. M. Johnson for making available his $(H_2O)_2Ar_n$ mass spectrum and for helpful discussions. The calculations were performed on computers in the University of Pittsburgh's Center for Molecular and Materials Simulations.

References and Notes

(1) Armbruster, M.; Haberland, H.; Schindler, H.-G. *Phys. Rev. Lett.* **1981**, *47*, 323.
(2) Ayotte, P.; Johnson, M. A. *J. Chem. Phys.* **1997**, *106*, 811.
(3) Desfrancois, C.; Bailon, B.; Schermann, J. P.; Arnold, S. T.; Hendricks, J. H.; Bowen, K. H. *J. Chem. Phys.* **1991**, *95*, 7760.
(4) Ayotte, P.; Weddle, G. H.; Bailey, G. G.; Johnson, M. A.; Vila, F.; Jordan, K. D. *J. Chem. Phys.* **1999**, *110*, 6268.
(5) Barnett, R. N.; Landman, U.; Cleveland, C. L.; Jortner, *J. Chem. Phys. Lett.* **1998**, *145*, 382.
(6) Kim, K. S.; Lee, S.; Kim, J.; Lee, Y. Y. *J. Am. Chem. Soc.* **1997**, *119*, 9329.
(7) Smith, D. M. A.; Smets, J.; Elkadi, Y.; Adamowicz, L. *J. Chem. Phys.* **1997**, *107*, 5788.
(8) Kelley, J. A.; Weddle, G. H.; Robertson, W. H.; Johnson, M. A. *J. Chem. Phys.* **2002**, *116*, 1201.
(9) Weber, J. M.; Kim, J.; Woronowicz, E. A.; Weddle, G. H.; Becker, I.; Cheshnovsky, O.; Johnson, M. A. *Chem. Phys. Lett.* **2001**, *339*, 337.
(10) Lee, H. M.; Lee, S.; Kim, K. S. *J. Chem. Phys.* **2003**, *119*, 187.
(11) Harberland, H.; Ludewigt, C.; Schindler, H. G.; Worsnop, D. R. *Phys. Rev. A* **1987**, *36*, 967.; Harberland, H.; Ludewigt, C.; Schindler, H. G.; Worsnop, D. R. *Z. Phys. A* **1985**, *320*, 151.
(12) Bowen, K. H.; Eaton, J. G. In *The Structure of Small Molecules and Ions*; Naaman, R., Vager, Z., Eds.; Plenum: New York, 1988; Arnold, S. T.; Eaton, J. G.; Patel-Misra, D.; Sarkas, H. W.; Bowen, K. H. In Ion and Cluster Ion Spectroscopy and Structure; Maier J. P., Ed.; Elsevier: Amsterdam, 1989.
(13) Bouteiller, Y.; Desfrancois, C.; Abdoul-Carime, H.; Shermann, J. P. *J. Chem. Phys.* **1996**, *105*, 6420.
(14) Coe, J. V.; Lee, G. H.; Eaton, J. G.; Arnold, S. T.; Sarkas, H. W.; Bowen, K. H.; Ludewigt, C.; Haberland, H.; Worsnop, D. R. *J. Chem. Phys.* **1990**, *92*, 3980.
(15) Wang, F.; Jordan, K. D. *Annu. Rev. Phys. Chem.* **2003**, *54*, 367−396.
(16) Fermi, E.; Teller, E. *Phys. Rev.* **1947**, *72*, 399.
(17) Turner, J. E.; Anderson, V. E.; Fox, K. **1968**, *174*, 81.
(18) Jordan, K. D. *Acc. Chem. Res.* **1979**, *12*, 36.
(19) Chipman, D. M. *J. Phys. Chem.* **1979**, *83*, 1657.
(20) Simons, J.; Jordan, K. D. *Chem. Rev.* **1987**, *87*, 535−556.
(21) Ayotte, P.; Johnson, M. A. Private communication.
(22) Corcelli, S. A.; Kelley, J. A.; Tully, J. C.; Johnson, M. A. *J. Phys. Chem. A* **2002**, *106*, 4872.
(23) Kroto, H. W.; Heath, J. R.; O'brien, S. C.; Curl, R. F.; Smalley, R. E. *Nature* **1985**, *318*, 162.
(24) Gutowski, M.; Jordan, K. D.; Skurski, P. *J. Phys. Chem. A* **1998**, *102*, 2624.
(25) Gutowski, M.; Jordan, K. D.; Boldyrev, A.; Simons, J.; Jordan, K. D. *Phys. Rev. A* **1996**, *54*, 1906.
(26) Simons, J.; Skurski, P. In *Theoretical Prospect of Negative Ions*; Kalcher, J., Ed.; Research Signpost, India, 2002.
(27) Dang, L. X.; Chang, T. M. *J. Chem. Phys.* **1997**, *106*, 8149.
(28) Cohen, R. C.; Saykally, R. J. *J. Chem. Phys.* **1993**, *98*, 6007.
(29) Space, B.; Coker, D. F.; Liu, Z. H.; Berne, B. J.; Martyna, G. *J. Chem. Phys.* **1992**, *97*, 2002.
(30) Shepard, A. C.; Beers, Y.; Klein, G. P.; Rothman, L. S. *J. Chem. Phys.* **1973**, *59*, 2254.
(31) Verhoeven, J.; Dymanus, A. *J. Chem. Phys.* **1970**, *52*, 3222.
(32) Wang, F.; Jordan, K. D. *J. Chem. Phys.* **2002**, *116*, 6973.
(33) Kirkpatrick, S.; Gelatt, C. D.; Vecchi, M. P. *Science* **1983**, *220*, 671.
(34) Press, W. H.; Flannery, B. P.; Teukolky, S. A.; Vetterling, W. T. In *Numerical recipes in C: The Art of Scientific Computing*, 2nd ed.; Cambridge University Press: New York, 1993.
(35) Ghayal, M. R.; Curotto, E. *J. Chem. Phys.* **1999**, *111*, 5522.
(36) Metropolis, N.; Rosenbluth, A. W.; Rosenbluth, M. N.; Teller, A. H.; Teller, E. *J. Chem. Phys.* **1953**, *21*, 1087.
(37) Gascón, J. A.; Hall, R. W.; Ludewigt, C.; Haberland, H. *J. Chem. Phys.* **2002**, *117*, 8391.
(38) Pople, J. A.; Head-Gordon, M.; Raghavachari, K. *J. Chem. Phys.* **1987**, *87*, 5968.
(39) Dunning, T. H., Jr. *J. Chem. Phys.* **1989**, *90*, 1007.
(40) Woon, D. E.; Dunning, T. H., Jr. *J. Chem. Phys.* **1993**, *98*, 1358.
(41) Kendall, R. A.; Dunning, T. H., Jr.; Harrison, R. J. *J. Chem. Phys.* **1992**, *96*, 6796.
(42) Johnson, M. Private communication.
(43) Weerasinghe, S.; Amar, F. G. *J. Chem. Phys.* **1993**, *98*, 4967.
(44) Frantz, D. D. *J. Chem. Phys.* **1995**, *102*, 3747.
(45) Frantz, D. D.; Freeman, D. L.; Doll, J. D. *J. Chem. Phys.* **1990**, *93*, 2769.